Proof-of-Principle Experiment for Testing Strong-Field Quantum Electrodynamics with Exotic Atoms: High Precision X-Ray Spectroscopy of Muonic Neon

T. Okumura[1,*,†] T. Azuma[1,‡] D. A. Bennett,[2] I. Chiu,[3] W. B. Doriese[2] M. S. Durkin,[2] J. W. Fowler,[2] J. D. Gard,[2] T. Hashimoto,[4] R. Hayakawa[5] G. C. Hilton,[2] Y. Ichinohe[6] P. Indelicato[7] T. Isobe[8] S. Kanda,[9] M. Katsuragawa,[10] N. Kawamura[9] Y. Kino[11] K. Mine,[10] Y. Miyake,[9] K. M. Morgan[2,12] K. Ninomiya,[3] H. Noda[13] G. C. O'Neil[2] S. Okada,[14,∥] K. Okutsu,[11] N. Paul[7] C. D. Reintsema,[2] D. R. Schmidt,[2] K. Shimomura,[9] P. Strasser[9] H. Suda,[5] D. S. Swetz[2] T. Takahashi,[10] S. Takeda,[10] S. Takeshita[9] M. Tampo,[9] H. Tatsuno[5] Y. Ueno,[1] J. N. Ullom,[2] S. Watanabe,[15] and S. Yamada[6]

[1]*Atomic, Molecular, and Optical Physics Laboratory, RIKEN, Wako 351-0198, Japan*
[2]*National Institute of Standards and Technology, Boulder, Colorado 80305, USA*
[3]*Institute for Radiation Sciences, Osaka University, Toyonaka, Osaka 560-0043, Japan*
[4]*Advanced Science Research Center (ASRC), Japan Atomic Energy Agency (JAEA), Tokai 319-1184, Japan*
[5]*Department of Physics, Tokyo Metropolitan University, Tokyo 192-0397, Japan*
[6]*Department of Physics, Rikkyo University, Tokyo 171-8501, Japan*
[7]*Laboratoire Kastler Brossel, Sorbonne Université, CNRS, ENS-PSL Research University,*
Collège de France, Case 74, 4, place Jussieu, 75005 Paris, France
[8]*RIKEN Nishina Center, RIKEN, Wako 351-0198, Japan*
[9]*High Energy Accelerator Research Organization (KEK), Tsukuba, Ibaraki 305-0801, Japan*
[10]*Kavli IPMU (WPI), The University of Tokyo, Kashiwa, Chiba 277-8583, Japan*
[11]*Department of Chemistry, Tohoku University, Sendai, Miyagi 980-8578, Japan*
[12]*Department of Physics, University of Colorado Boulder, Boulder, Colorado 80309, USA*
[13]*Department of Earth and Space Science, Osaka University, Toyonaka, Osaka 560-0043, Japan*
[14]*Engineering Science Laboratory, Chubu University, Kasugai, Aichi 487-8501, Japan*
[15]*Department of Space Astronomy and Astrophysics, Institute of Space and Astronautical Science (ISAS),*
Japan Aerospace Exploration Agency (JAXA), Sagamihara, Kanagawa 252-5210, Japan

To test bound-state quantum electrodynamics (BSQED) in the strong-field regime, we have performed high precision x-ray spectroscopy of the $5g-4f$ and $5f-4d$ transitions (BSQED contribution of 2.4 and 5.2 eV, respectively) of muonic neon atoms in the low-pressure gas phase without bound electrons. Muonic atoms have been recently proposed as an alternative to few-electron high-Z ions for BSQED tests by focusing on circular Rydberg states where nuclear contributions are negligibly small. We determined the $5g_{9/2}-4f_{7/2}$ transition energy to be $6297.08 \pm 0.04(\text{stat}) \pm 0.13(\text{syst})$ eV using superconducting transition-edge sensor microcalorimeters (5.2–5.5 eV FWHM resolution), which agrees well with the most advanced BSQED theoretical prediction of 6297.26 eV.

Quantum electrodynamics (QED) is one of the most precisely examined theories in physics. In hydrogen, the QED correction to the $1s$–$2s$ transition energy is 8 172 770.4(2.1) kHz corresponding to 3.3 ppm of the total energy [1], which was measured with ∼10 Hz accuracy [2,3]. The calculated value is in excellent agreement with experiment, the difference being 0.1(2.1) kHz. The QED contribution to the transition energy increases in general with Z^2 (Z, nuclear charge). However, it is known that the theoretical approach using a perturbative expansion with αZ ($\alpha \approx 1/137$, fine-structure constant) does not converge at high Z. Thus, a comparison between experimental and theoretical bound-state QED (BSQED) under strong fields is of utmost necessity. It has been explored intensively with highly charged ions (HCIs); see Ref. [4] for a recent review.

The most precise measurement of the ground-state Lamb shift in high-Z systems is so far limited to an accuracy of 1% [5]. Moreover, HCI studies face a severe difficulty, i.e., the non-negligible contribution of the finite nuclear size (FNS), and its uncertainties often overwhelm the second-order BSQED contribution [4,6]. Thus, tests of BSQED in the strong-field regime are still in their infancy.

Muonic atoms, where a negative muon is captured onto the atomic orbitals, replacing an electron, provide a unique window into strong electric field atomic physics because muons are 207 times closer to the nucleus than electrons and thus probe high Coulomb fields. When a muon is captured by an atom, it experiences a cascading deexcitation process by Auger electron emission, which results in the peeling off of the bound electrons of the atom.

The cascade is followed by photon emission in the x-ray regime [7]. Muonic atoms have been of great interest for measuring fundamental physics parameters and searching for beyond-standard-model physics [8–12].

A negative muon in a muonic atom with a high-Z nucleus is exposed to the strong electric field of the nucleus, which also makes it a good probe to explore BSQED in the strong fields. In this simple exotic atom, the leading-order BSQED correction to the x-ray transitions is the vacuum polarization (VP), i.e., polarization of virtual electron-positron pairs in the muon-nucleus field, followed by the self-energy, which is the reverse order compared to ordinary atoms consisting of an electron and a nucleus. This is because, when the muon comes so close to the nucleus, generally less than the electron's Compton wavelength, the muon would feel "bare" nuclear charge freeing from "polarization" charge, resulting in enhanced VP [13]. As the ensemble of atomic states in muonic atoms are found in a higher field regime than their normal electronic counterparts, and this simple two-body system can be calculated with high precision, these systems are ideal probes of BSQED and particularly of the VP effect. Recently, we theoretically proposed the advantages of exotic atoms over HCIs for BSQED tests in Ref. [14]. A region of suitable transitions may be found between high-n_μ circular Rydberg states (n_μ, the principal quantum number of the muon orbitals) where nuclear contributions to the transition energies are vanishing, while BSQED contributions remain large, creating a unique opportunity to cleanly probe strong-field BSQED.

The history of BSQED tests using muonic and other exotic atoms can be traced back to the 1970s [13]. Unfortunately, all of these experiments employed solid-state targets, and the resulting screening effects from unavoidable recaptured electrons, in addition to the use of low-n_μ transitions with large FNS corrections, limited the sensitivity to BSQED effects in the transition energies. After the recognition of the electron refilling problem, particularly in πMg measurements [15,16], muonic x-ray measurements using gas targets were explored. Pressure effects on the muon cascade and the transition energies were intensively studied in [17–22]. Kirch *et al.* concluded that a pressure below 0.1 atm is necessary to completely isolate μNe during the muon cascade [22], where such low-target-density conditions preclude the use of a crystal spectrometer.

Precision measurements of pionic x rays with gas targets employing a cyclotron trap and a crystal spectrometer have been carried out at relatively high pressures around 1 atm [23]. In the updated experiment by Trassinelli *et al.* [24], the pionic x rays from πN were measured together with the muonic x rays from μO, which were located close to the target pionic line and used as a reference for energy calibration under the assumption that the calculated BSQED contribution was correct. They could, in principle,

achieve a QED test with a 1%-level accuracy by calibrating the μO lines against the Cu $K\alpha$ line, which was measured simultaneously as a stability monitor, although they did not discuss this aspect.

We aim to test strong-field BSQED by muonic x-ray spectroscopy with high resolution under the condition that there are no remaining electrons in the muonic atoms. To prepare the clean two-body system, two requirements are crucial. First, one must be sure of the full stripping of bound electrons via the Auger process during the muon deexcitation, which requires a nucleus of relatively low atomic number Z. Furthermore, electron refilling from neighboring atoms or molecules has to be avoided, leading to the second requirement of the isolated condition of the muonic atom, i.e., formation in a low-pressure gas.

To achieve a high-resolution and high-detection efficiency for the muonic x-ray detection under such a low-pressure condition, we took full advantage of multipixel transition-edge sensor (TES) superconducting x-ray calorimeters. The broadband feature of the TES detector makes it possible to measure different muonic x-ray peaks simultaneously. This allowed us to measure both the targeted peak energy for the BSQED test and other peak energies for directly evaluating the number of the remaining electrons in the muonic atom.

The Materials and Life Science Experimental Facility (MLF) at J-PARC provides the necessary intense pulsed negative muon beams with energies down to 58 keV (3.5 MeV/c) [25]. This enables us to stop isolated muons directly at high rates in low-density gas targets. We already have demonstrated excellent performance of the TES detector for accelerator-based experiments [26–28].

In this Letter, using the TES detector, we report precision measurements of muonic x rays from completely ionized μNe isolated in a dilute gas and compare the results with updated stringent BSQED theory. We selected the muonic x rays of the $5g$–$4f$ and $5f$–$4d$ transitions of μNe as targets for measurements because (1) the transitions include 2.4 and 5.2 eV BSQED contributions (4–8×10^{-4} relative to the transition energy) which are resolvable by the TES detector at the 0.1 eV level, (2) the FNS contribution is negligibly small, and (3) bound electrons are absent. We also exploit a muonic x-ray peak from $7h$–$5g$ and $7g$–$5f$ transitions, which was measured simultaneously with the target peak owing to the broad dynamic range of the TES detector, to confirm the absence of remaining K-shell electrons at $n_\mu = 5$.

The experiment was carried out at the D2 beamline of the MLF at J-PARC [25]. Details of the setup were described in previous papers [27,29,30]. The major differences from the previous experiment using a metal-foil target [27] are that a gas target was used, and careful calibration procedures were implemented notably to correct the small but significant temporal energy shifts under the pulsed-mode operation of the muon beam. We prepared the low-pressure

Ne gas target as low as 0.1 atm at room temperature and studied the pressure dependence. The neon gas contained ^{20}Ne and ^{22}Ne with the natural isotopic abundances of 90.48% and 9.25%. The muons were delivered in a double-pulse structure containing $\sim 10^4$ muons per double pulse with a repetition rate of 25 Hz. The muon momentum values were optimized to 20.5, 20.5, and 21.5 MeV/c at neon pressures of 0.1, 0.4, and 0.9 atm, respectively, to maximize the number of stopped muons within the field of view of the detector. Typical count rates of muonic x rays on the whole detector array were 1–3 counts per second. We employed a 240-pixel TES array developed by the National Institute of Standards and Technology [31]. For accurate online energy calibration, we simultaneously monitored characteristic K x rays from Cr, Co, and Cu produced by an x-ray generator [27]. Energy calibration of each TES pixel was carried out by following the procedure of Refs. [32,33].

We observed the energy shift originating from the pulsed-mode operation of the muon beam, which can be understood by thermal crosstalk resulting from high-energy charged particles accompanying the muon beam injection [30]. When charged particles, produced by muon decay or nuclear capture, or scattered by the Ne gas, hit the TES pixel array, a large fraction of the deposited energy is converted into heat in the Si frame of the TES pixel, causing a change in the raw TES waveform that results from the x-ray detection. The energy shifts in the observed region were roughly 0.3, 0.4, and 0.5 eV at pressures of 0.1, 0.4, and 0.9 atm. These shifts are corrected by measuring the peak-energy deviation of the calibration K x-ray peaks as a function of the detection time with respect to the pulsed muon beam injection, as well as employing a small temperature rise observed in the surrounding TES pixels (see the details in the Supplemental Material [34]). We evaluated the accuracy of this correction from experimental results using a Fe foil target. From a comparison of peak positions of Fe $K\alpha$ x rays, which are emitted only at the muon-beam injection and affected by the crosstalk effect, to the reference value [37,38], we confirmed that the energy shifts are properly corrected with an error below 0.11 eV.

We obtained x-ray spectra by summing up those from all TES pixels under normal operation after selecting the events within a specific time window to extract the muon-beam induced signals [29]. The x-ray spectrum at a pressure of 0.9 atm after correction for the thermal crosstalk is shown in Fig. 1. A muonic x-ray peak from the 5–4 transition of μNe is clearly seen at around 6300 eV. The 7–5 transition peak of μNe is also identified at 5480 eV.

The typical expanded spectrum of the 5–4 transition peak at a pressure of 0.1 atm is shown in Fig. 2. To determine the transition energies, the muonic x-ray peaks were fitted with the curves obtained by a convolution of the line shape model with the TES response function using the maximum likelihood method. We also employed a
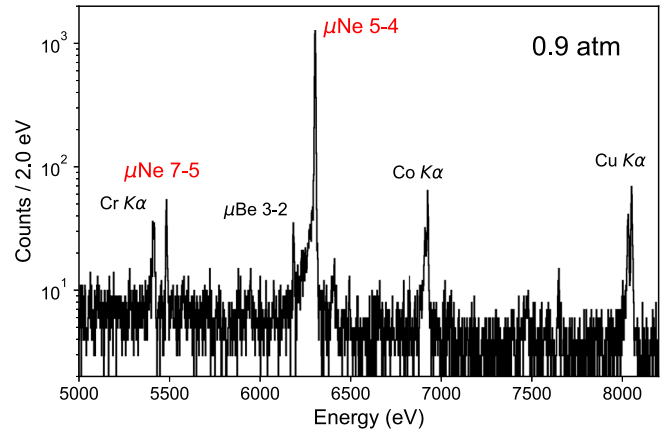
FIG. 1. An x-ray spectrum from 5−4 and 7−5 transitions of μNe at a pressure of 0.9 atm. A muonic x-ray peak from μBe produced at the Be x-ray window in front of the TES detector, along with small calibration x-ray peaks, are also identified.

Bayesian analysis program [39,40] to check correlations between the fitting parameters. The TES response function is a Gaussian function accompanied by a low-energy tail, which originates from the trapping of heat carriers in the Bi absorber [41]. The function has three parameters: the energy resolution and the fraction and length of the low-energy tail. The energy resolution was evaluated by fitting the μNe peak. We fixed the two tail parameters obtained from the calibration K x-ray peaks under the off-beam condition.

The observed μNe peak is a sum of contributions from two isotopes, ^{20}Ne and ^{22}Ne. Each isotopic component contains three $5g-4f$ and three weaker $5f-4d$ transitions.
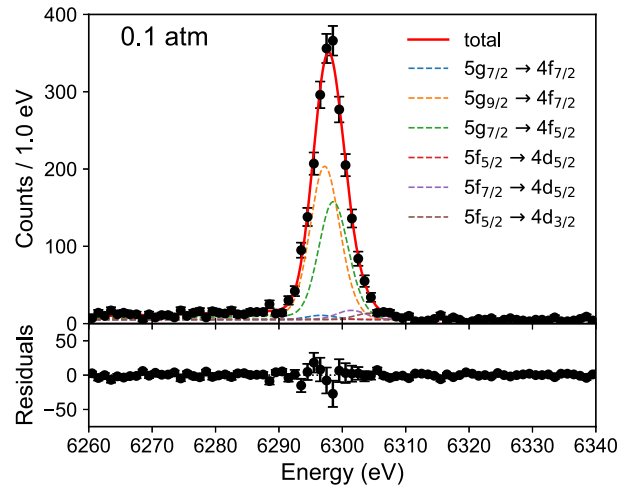
FIG. 2. X-ray spectra from 5−4 transitions of μNe at a pressure of 0.1 atm. The fitted profiles obtained by summing up μ^{20}Ne and μ^{22}Ne contributions are also shown with residual errors. The fitting is carried out by using three spectra at pressures of 0.1, 0.4, and 0.9 atm simultaneously, and the reduced χ^2 (number of degrees of freedom, 284) for the total fitting is evaluated to be 1.26.

TABLE I.   Theoretically calculated energies of the μ^{20}Ne 5−4 transitions with BSQED (vacuum polarization from Uehling effect, self-energy, and higher-order contributions), FNS and recoil contributions, and relative intensities among fine-structure-resolved transition. The total transition energies contain all BSQED, FNS, and recoil shifts. The relative intensities are obtained assuming statistical distribution among fine-structure levels. We also list the energy shifts due to one K-shell electron screening. The uncertainties of the calculations are in the order of the last digit of each value.

Initial state	Final state	Transition energy (eV)						Relative intensity	One K-shell e^- energy shift (eV)
		Total transition energy	Vacuum polarization	Self-energy	QED order $\geq \alpha^2$	FNS	Recoil		
$5g_{9/2}$	$4f_{7/2}$	6297.261 91	2.338 03	−0.001 52	0.022 97	0.000 31	0.004 95	1.0000	−1.251 98
$5g_{7/2}$	$4f_{7/2}$	6296.664 27	2.337 75	−0.002 91	0.022 97	0.000 31	0.004 97	0.0286	−1.251 63
$5g_{7/2}$	$4f_{5/2}$	6298.611 92	2.340 51	0.001 60	0.022 95	0.000 31	0.004 91	0.7715	−1.251 96
$5f_{7/2}$	$4d_{5/2}$	6301.432 65	5.144 45	−0.003 45	0.044 56	0.001 37	0.005 16	1.0000	−1.618 66
$5f_{5/2}$	$4d_{5/2}$	6300.435 36	5.143 01	−0.005 74	0.044 55	0.001 37	0.005 19	0.0503	−1.618 05
$5f_{5/2}$	$4d_{3/2}$	6304.340 99	5.156 41	0.003 23	0.044 61	0.001 45	0.005 07	0.6991	−1.618 76

The theoretical values of the transition energies, QED, FNS, and recoil shifts, and relative intensity of μ^{20}Ne are listed in Table I (transition energies for μ^{22}Ne are found in the Supplemental Material [34]). These results were obtained by BSQED calculations that include first- and second-order QED corrections, the full Breit interaction, all-order retardation effects, and the FNS contributions using the MCDFGME code [42–45]. This code can compute the above effects for muonic atoms with an arbitrary number of remaining electrons. The energy shifts due to the one K-shell electron screening are −1.25 and −1.62 eV for the $5g$−$4f$ and $5f$−$4d$ transitions, respectively. As seen in Table I, the theoretical calculation predicts that vacuum polarization dominates the shifts for all transitions that contribute to the observed line. Other contributions are more than 2 orders of magnitude smaller than vacuum polarization. The transition energy differences within the fine-structure-resolved levels are mainly explained by the spin-orbit interaction in the Dirac equation.

Transitions with different total angular momenta for the $5g$−$4f$ and $5f$−$4d$ transitions are not resolved by the detector. Thus, to fit the data, we allowed the energy of the most intense transition, i.e., $5g_{9/2}$−$4f_{7/2}$, to vary and fixed the transition energy differences between the fine-structure levels and between $5g$−$4f$ and $5f$−$4d$ transitions to the calculated values in Table I. The relative intensities of the fine-structure levels are fixed to their statistical population. On the other hand, the intensity ratio between the $5f$−$4d$ and $5g$−$4f$ transitions, R_{5f-4d}, is affected by the details of the cascade deexcitation process. By also allowing R_{5f-4d} to vary, we arrived at five fitting parameters: $5g_{9/2}$−$4f_{7/2}$ transition energy for μ^{20}Ne, intensity ratio R_{5f-4d}, total intensity, a constant background, and the energy resolution. Note that we fixed the energy differences and the relative intensities between μ^{20}Ne and μ^{22}Ne to the calculated values and the natural isotope abundance, respectively. The fitted result is shown in Fig. 2 with the residual error. With

regard to the energy resolution, the experimental widths (FWHM) are 5.18(14), 5.50(12), and 5.51(11) eV at pressures of 0.1, 0.4, and 0.9 atm, respectively, whereas the resolutions for the beam-off condition are 5.0–5.2 eV at the Co $K\alpha$ peak. The obtained R_{5f-4d} is 0.059(9), which is consistent with the well-known behavior that the deexcitation cascade dominantly proceeds via the transitions between the levels of $\ell_\mu = n_\mu - 1$.

The experimental $5g_{9/2}$−$4f_{7/2}$ transition energies for μ^{20}Ne are given in Table II and shown in Fig. 3. Associated uncertainties are also listed in Table II. We consider three sources of systematic uncertainties: energy calibration, estimation of the low-energy tail of the TES response function, and the thermal crosstalk correction. (1) The calibration uncertainty of the TES detector is mainly determined by errors accompanying the interpolation between the anchor points. We evaluated the net uncertainty of our calibration by evaluating the peak energy of the Fe $K\alpha$ line. Our obtained energy is 6404.01(7) eV, and we employed 0.07 eV as the net uncertainty. The peak energy agrees well with the reported energy of 6404.0062(99) eV, which was determined more precisely with a single-crystal diffractometer [38]. (2) The tail parameters might change from the off-beam values due

TABLE II.   The experimental $5g_{9/2}$-$4f_{7/2}$ transition energies for μ^{20}Ne and associated uncertainties.

Transition energy and uncertainties (eV)	$5g_{9/2}$−$4f_{7/2}$		
	0.1 atm	0.4 atm	0.9 atm
Measured energy	6297.13	6297.06	6297.05
Statistical error	0.07	0.06	0.06
Systematic error: Total	0.13	0.13	0.13
(1) Calibration	0.07	0.07	0.07
(2) Low-energy tail	0.01	0.02	0.01
(3) Thermal crosstalk	0.11	0.11	0.11
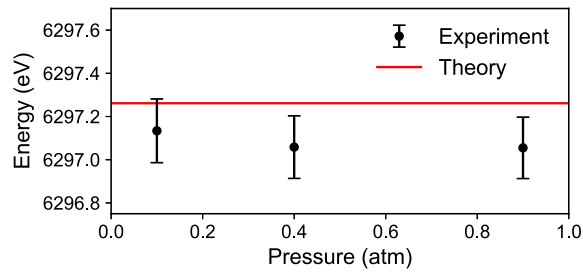
FIG. 3. Comparison of the obtained μ^{20}Ne $5g_{9/2} - 4f_{7/2}$ transition energies at pressures of 0.1, 0.4, and 0.9 atm with the theoretical value (red solid line).

to the thermal crosstalk. We tried fitting without fixing them and obtained the related errors. (3) Uncertainty due to the crosstalk correction is below 0.11 eV as already described. Thus, the total systematic errors were 0.13 eV, which were governed mainly by the calibration uncertainty and the crosstalk correction.

In order to evaluate contribution from remaining K-shell electrons in μNe, we monitored the muonic x rays from the 7–5 transitions at around 5480 eV. In a sharp contrast to the 5–4 transitions, their energy shift due to the K-shell electron screening is expected to be much larger, i.e., -6.93 and -7.68 eV for $7h–5g$ and $7g–5f$ transitions, respectively, while the BSQED contribution is about 6 times smaller (see the Supplemental Material [34]). If μNe with one K-shell electron at $n_\mu = 7$ exists, the satellite structure would appear at the low-energy side of the main peak. We fitted the observed 7–5 spectrum considering the satellite contribution with a new fitting parameter f_{1e}, a fraction of μNe with one K electron. The low number of counts in the peak prevents a determination of the relative intensity between the $7g–5f$ and $7h–5g$ peaks, R_{7g-5f}, by fitting. We employed instead the values $0.20 \leq R_{7g-5f} \leq 0.37$, obtained from a muon cascade simulation by the Akylas-Vogel code [46]. Details of the simulation are discussed in the Supplemental Material [34]. The fitting result for the K-electron contribution is $f_{1e} = 0.00^{+0.08}_{-0.00}$ for all R_{7g-5f} values considered here, which means that the μNe atoms can be considered to be fully ionized. This result is also consistent from the viewpoint of the timescale of the relevant processes; the muon cascade proceeds within 10^{-10} s at largest [20], while the time between charge transfer collisions of μNe with the surrounding Ne is in the range of 10^{-9} s [47].

In summary, we experimentally determined the $5g_{9/2} - 4f_{7/2}$ transition energy of μ^{20}Ne to be 6297.08 ± 0.04(stat) ± 0.13(syst) eV by averaging the data at pressures of 0.1, 0.4, and 0.9 atm. The statistical error is evaluated by the weighted average. This value agrees well with the most advanced BSQED theoretical prediction of 6297.26 eV. We also experimentally confirmed full ionization of μNe from the 7–5 transition peak, which was

possible thanks to the broadband feature of the TES detector. We obtained, for the first time, the QED vacuum polarization contribution to this transition with an accuracy of 5.8%, for the fully ionized exotic hydrogenlike two-body system under such low-pressure conditions free from both the effect of the FNS ($\sim 0.01\%$ relative to the VP contribution) and the K-shell electron shift, while previous reports on BSQED tests by muonic atoms in solids have not satisfied these conditions [48–51]. Thus, the present measurement is regarded to be a significant milestone for strong-field BSQED tests. Presently, we are preparing the measurements of larger QED contribution (~ 100 eV) from the 4–3 transitions (44 keV) of μAr by introducing newly developed TES microcalorimeters covering the energy region up to 50 keV [52], which is not practically accessible with a crystal spectrometer.

* tokumura@tmu.ac.jp
† Present address: Department of Chemistry, Tokyo Metropolitan University, Hachioji, Tokyo 192-0397, Japan.
‡ toshiyuki-azuma@riken.jp
‖ sokada@isc.chubu.ac.jp

[1] V. A. Yerokhin, K. Pachucki, and V. Patkóš, Ann. Phys. (Amsterdam) 531, 1800324 (2019).
[2] C. G. Parthey, A. Matveev, J. Alnis, B. Bernhardt, A. Beyer, R. Holzwarth, A. Maistrou, R. Pohl, K. Predehl, T. Udem et al., Phys. Rev. Lett. 107, 203001 (2011).
[3] A. Matveev, C. G. Parthey, K. Predehl, J. Alnis, A. Beyer, R. Holzwarth, T. Udem, T. Wilken, N. Kolachevsky, M. Abgrall et al., Phys. Rev. Lett. 110, 230801 (2013).
[4] P. Indelicato, J. Phys. B 52, 232001 (2019).

[5] A. Gumberidze, T. Stöhlker, D. Banaś, K. Beckert, P. Beller, H. F. Beyer, F. Bosch, S. Hagmann, C. Kozhuharov, D. Liesen et al., Phys. Rev. Lett. 94, 223001 (2005).

[6] A. V. Volotka, D. A. Glazov, G. Plunien, and V. M. Shabaev, Ann. Phys. (Berlin) 525, 636 (2013).

[7] D. Horváth, in Handbook of Nuclear Chemistry, 2nd ed., edited by A. Vértes, S. Nagy, Z. Klencsár, R. G. Lovas, and F. Rösch (Springer, Boston, 2011), pp. 1485–1513.

[8] R. Pohl, A. Antognini, F. Nez, F. D. Amaro, F. Biraben, J. M. R. Cardoso, D. S. Covita, A. Dax, S. Dhawan, L. M. P. Fernandes et al., Nature (London) 466, 213 (2010).

[9] A. Antognini, F. Nez, K. Schuhmann, F. D. Amaro, F. Biraben, J. M. R. Cardoso, D. S. Covita, A. Dax, S. Dhawan, M. Diepold et al., Science 339, 417 (2013).

[10] R. Pohl, F. Nez, L. M. P. Fernandes, F. D. Amaro, F. Biraben, J. M. R. Cardoso, D. S. Covita, A. Dax, S. Dhawan, M. Diepold et al., Science 353, 669 (2016).

[11] J.-P. Karr, D. Marchand, and E. Voutier, Nat. Rev. Phys. 2, 601 (2020).

[12] J. J. Krauth, K. Schuhmann, M. A. Ahmed, F. D. Amaro, P. Amaro, F. Biraben, T.-L. Chen, D. S. Covita, A. J. Dax, M. Diepold et al., Nature (London) 589, 527 (2021).

[13] E. Borie and G. A. Rinker, Rev. Mod. Phys. 54, 67 (1982).

[14] N. Paul, G. Bian, T. Azuma, S. Okada, and P. Indelicato, Phys. Rev. Lett. 126, 173001 (2021).

[15] B. Jeckelmann, T. Nakada, W. Beer, G. de Chambrier, O. Elsenhans, K. L. Giovanetti, P. F. A. Goudsmit, H. J. Leisi, A. Rüetschi, O. Piller et al., Phys. Rev. Lett. 56, 1444 (1986).

[16] B. Jeckelmann, P. Goudsmit, and H. Leisi, Phys. Lett. B 335, 326 (1994).

[17] P. Ehrhart, F. J. Hartmann, E. Köhler, and H. Daniel, Z. Phys. A 311, 259 (1983).

[18] R. Bacher, D. Gotta, L. M. Simons, J. Missimer, and N. C. Mukhopadhyay, Phys. Rev. Lett. 54, 2087 (1985).

[19] R. Jacot-Guillarmod, F. Bienz, M. Boschung, C. Piller, L. A. Schaller, L. Schellenberg, H. Schneuwly, and D. Siradovic, Phys. Rev. A 37, 3795 (1988).

[20] R. Bacher, P. Blüm, D. Gotta, K. Heitlinger, M. Schneider, J. Missimer, and L. M. Simons, Phys. Rev. A 39, 1610 (1989).

[21] L. Simons, D. Abbot, B. Bach, R. Bacher, A. Badertscher, P. Blüm, P. DeCecco, J. Eades, J. Egger, K. Elsener et al., Nucl. Instrum. Methods Phys. Res., Sect. B 87, 293 (1994).

[22] K. Kirch, D. Abbott, B. Bach, P. Hauser, P. Indelicato, F. Kottmann, J. Missimer, P. Patte, R. T. Siegel, L. M. Simons et al., Phys. Rev. A 59, 3375 (1999).

[23] S. Lenz, G. Borchert, H. Gorke, D. Gotta, T. Siems, D. Anagnostopoulos, M. Augsburger, D. Chatellard, J. Egger, D. Belmiloud et al., Phys. Lett. B 416, 50 (1998).

[24] M. Trassinelli, D. Anagnostopoulos, G. Borchert, A. Dax, J.-P. Egger, D. Gotta, M. Hennebach, P. Indelicato, Y.-W. Liu, B. Manil et al., Phys. Lett. B 759, 583 (2016).

[25] W. Higemoto, R. Kadono, N. Kawamura, A. Koda, K. Kojima, S. Makimura, S. Matoba, Y. Miyake, K. Shimomura, and P. Strasser, Quantum Beam Sci. 1, 11 (2017).

[26] S. Okada, D. A. Bennett, C. Curceanu, W. B. Doriese, J. W. Fowler, J. D. Gard, F. P. Gustafsson, T. Hashimoto, R. S. Hayano, S. Hirenzaki et al., Prog. Theor. Exp. Phys. 2016, 091D01 (2016).

[27] T. Okumura, T. Azuma, D. A. Bennett, P. Caradonna, I. Chiu, W. B. Doriese, M. S. Durkin, J. W. Fowler, J. D. Gard, T. Hashimoto et al., Phys. Rev. Lett. 127, 053001 (2021).

[28] T. Hashimoto, S. Aikawa, T. Akaishi, H. Asano, M. Bazzi, D. A. Bennett, M. Berger, D. Bosnar, A. D. Butt, C. Curceanu et al., Phys. Rev. Lett. 128, 112503 (2022).

[29] S. Okada, T. Azuma, D. A. Bennett, P. Caradonna, W. B. Doriese, M. S. Durkin, J. W. Fowler, J. D. Gard, T. Hashimoto, R. Hayakawa et al., J. Low Temp. Phys. 200, 445 (2020).

[30] T. Okumura, T. Azuma, D. A. Bennett, P. Caradonna, I.-H. Chiu, W. B. Doriese, M. S. Durkin, J. W. Fowler, J. D. Gard, T. Hashimoto et al., IEEE Trans. Appl. Supercond. 31 (2021).

[31] W. B. Doriese, P. Abbamonte, B. K. Alpert, D. A. Bennett, E. V. Denison, Y. Fang, D. A. Fischer, C. P. Fitzgerald, J. W. Fowler, J. D. Gard et al., Rev. Sci. Instrum. 88, 053108 (2017).

[32] J. W. Fowler, B. K. Alpert, D. A. Bennett, W. B. Doriese, J. D. Gard, G. C. Hilton, L. T. Hudson, Y.-I. Joe, K. M. Morgan, G. C. O'Neil et al., Metrologia 54, 494 (2017).

[33] J. W. Fowler, G. C. O'Neil, B. K. Alpert, D. A. Bennett, E. V. Denison, W. B. Doriese, G. C. Hilton, L. T. Hudson, Y.-I. Joe, K. M. Morgan et al., Metrologia 58, 015016 (2021).

[34] See Supplemental Material at http://link.aps.org/supplemental/10.1103/PhysRevLett.130.173001 for details of the muon-stopping simulation with GEANT4 [35], the calibration function, the procedure of the thermal crosstalk correction, which includes Ref. [36], the theoretical muonic x-ray energies, the experimental relative peak intensities, the cascade simulation, and possibility of electron recapture.

[35] GEANT4, https://geant4.web.cern.ch.

[36] J. W. Fowler, B. K. Alpert, W. B. Doriese, Y. I. Joe, G. C. O'Neil, J. N. Ullom, and D. S. Swetz, J. Low Temp. Phys. 184, 374 (2016).

[37] G. Hölzer, M. Fritsch, M. Deutsch, J. Härtwig, and E. Förster, Phys. Rev. A 56, 4554 (1997).

[38] R. D. Deslattes, E. G. Kessler, P. Indelicato, L. de Billy, E. Lindroth, and J. Anton, Rev. Mod. Phys. 75, 35 (2003).

[39] M. Trassinelli, Nucl. Instrum. Methods Phys. Res., Sect. B 408, 301 (2017).

[40] M. Trassinelli, Proceedings 33, 14 (2019).

[41] H. Tatsuno, W. B. Doriese, D. A. Bennett, C. Curceanu, J. W. Fowler, J. Gard, F. P. Gustafsson, T. Hashimoto, R. S. Hayano, J. P. Hays-Wehle et al., J. Low Temp. Phys. 184, 930 (2016).

[42] J. V. Mallow, J. P. Desclaux, and A. J. Freeman, Phys. Rev. A 17, 1804 (1978).

[43] J. P. Santos, F. Parente, S. Boucard, P. Indelicato, and J. P. Desclaux, Phys. Rev. A 71, 032501 (2005).

[44] M. Trassinelli and P. Indelicato, Phys. Rev. A 76, 012510 (2007).

[45] P. Indelicato, Phys. Rev. A 87, 022501 (2013).

[46] V. R. Akylas and P. Vogel, Comput. Phys. Commun. **15**, 291 (1978).

[47] K. Suzuki, K. Okuno, and N. Kobayashi, Phys. Scr. T **73**, 172 (1997).

[48] R. Eichler, B. Aas, W. Beer, I. Beltrami, P. Ebersold, T. v. Ledebur, H. J. Leisi, W. W. Sapp, J. C. Dousse, J. Kern *et al.*, Phys. Lett. **76B**, 231 (1978).

[49] B. Aas, W. Beer, I. Beltrami, P. Ebersold, R. Eichler, T. V. Ledebur, H. J. Leisi, W. Ruckstuhl, W. W. Sapp, A. Vacchi *et al.*, Nucl. Phys. **A375**, 405 (1982).

[50] W. Ruckstuhl, B. Aas, W. Beer, I. Beltrami, F. W. N. de Boer, K. Bos, P. F. A. Goudsmit, U. Kiebele, H. J. Leisi, G. Strassner *et al.*, Phys. Rev. Lett. **49**, 859 (1982).

[51] I. Beltrami, B. Aas, W. Beer, P. Ebersold, R. Eichler, P. F. A. Goudsmit, M. Guanziroli, T. v. Ledebur, H. J. Leisi, W. Ruckstuhl *et al.*, Nucl. Phys. **A429**, 381 (1984).

[52] D. Yan, J. Weber, K. Morgan, A. Wessels, D. Bennett, C. Pappas, J. Mates, J. Gard, D. Becker, J. Fowler *et al.*, IEEE Trans. Appl. Supercond. **31** (2021).